Chemical Science

Accepted Manuscript

This article can be cited before page numbers have been issued, to do this please use: Y. Qin, V. Sethuraman, S. Choi, R. Gonzalez, C. Chen, L. Cheng, C. Luo and T. Gao, *Chem. Sci.*, 2025, DOI: 10.1039/D5SC04532K.

ROYAL SOCIETY OF CHEMISTRY

rsc.li/chemical-science

View Article Online
DOI: 10.1039/D5SC04532K

Conjugation effect of amine molecules in non-aqueous Mg redox flow batteries

Yunan Qin [a], Vaidyanathan Sethuraman [b], Seong-Gyu Choi [a], Richard Gonzalez [a], Chengxiang Chen [c], Lei Cheng [b], Chao Luo [c]*, Tao Gao [a]*

[a] Department of Chemical Engineering, University of Utah, Salt Lake City, UT, USA

[b] Chemical Sciences Division, Oak Ridge National Laboratory, Oak Ridge, TN, USA

[c] Department of Chemical, Environmental and Materials Engineering, University of Miami, Coral Gables, FL, USA

*Corresponding: taogao@chemeng.utah.edu; cxl1763@miami.edu.

Abstract

Nonaqueous magnesium redox flow batteries (Mg RFBs) are attractive for low-cost, high-energy-density and long-cycle-life stationary energy storage applications. However, state-of-the-art cathode redox-active molecules suffer from low solubility and low redox potential. Herein, we screened a range of cathode redox-active molecules and identified amine molecules as optimal to couple with Mg anode. The properties of amine derivatives and their performances were collected to establish the correlation between molecular structures and electrochemical performances. The results confirm that the redox potential and solubility of these amine molecules are influenced by π-conjugated and non-conjugated structures of amine derivatives. Density functional theory (DFT) simulations and inverse aromatic fluctuation index (FLU^{-1}) verified that the conjugation plays an important role in stabilizing the molecule and increasing its redox potential. Notably, tris[4-(diethylamino)phenyl]amine (TDPA) achieves the highest theoretical energy density (~120 Wh/L) due to its high solubility (~0.9 M) and voltage (~2.5 V vs. Mg/Mg^{2+}). The study also demonstrates

View Article Online
DOI: 10.1039/D5SC04532K

that ether solvents are crucial for stable, high-solubility catholytes, while bulk anions do not affect the redox potential of these *p*-type molecules. In a Mg-amine RFB configuration, the battery delivered 2.50 V, 106.5 mAh/g specific discharge capacity, 90.74% initial Coulombic efficiency, and 93.88% capacity retention after 150 cycles.

Keywords

flow battery, magnesium anode, amine catholyte, non-aqueous electrolyte

Introduction

Owing to the limited resources and negative environmental impacts (CO_2 emissions) of fossil fuel, it is necessary to explore renewable energy sources for electricity production.[1,2] Such a transition requires efficient energy storage solutions to address the intermittency of renewable energy. Among different storage technologies, electrochemical energy storage (or batteries) has gained broad attention.[3,4] According to the International Energy Agency (IEA), energy storage must grow six-fold to triple the global renewable energy capacity by 2030, where batteries will drive 90% of this expansion.[5] This increase reflects the importance of electrochemical storage. Li-ion batteries (LIBs) are the most studied and deployed energy storage technology, while they suffer from supply chain challenges and high cost.[6,7] Therefore, there is an urgent need for alternative energy storage technologies given huge demands for affordable energy storage for grid resilience.

Redox flow batteries (RFBs) have the potential to meet these requirements. The redox-active molecules are dissolved into liquid electrolytes and pumped through external tanks to electrodes for electrochemical reactions.[8] This unique cell structure benefits readily and independently scalable energy and power, as well as other advantages such as fast solution reaction kinetics,

View Article Online
DOI: 10.1039/D5SC04532K

minimal phase transformation, long cycle life and safety.[9] Based on the solvent used in the electrolyte, RFBs can be divided into aqueous RFBs and nonaqueous RFBs. To date, the commercial flow batteries are aqueous, such as all vanadium batteries and hybrid zinc batteries.[10,11] However, the operation voltage of these aqueous RFBs is usually below 1.5 V due to electrochemical water splitting.[12] The low voltage limits the power density and energy density of aqueous RFBs. Moreover, the use of high-cost and toxic materials such as vanadium in these aqueous RFBs poses challenges to the environment and energy sustainability. To address these challenges and achieve high-power-density and high-energy-density energy storage systems, developing high-voltage nonaqueous RFBs offer opportunities.[13]

Among various nonaqueous RFBs, Mg RFBs stand out.[14–16] The motivation in novel Mg RFBs roots in two unique advantages of Mg electrochemistry: (1) high voltage and energy density. Mg anodes have low redox potential (-2.37 V vs. standard hydrogen electrode) and a high volumetric capacity (3833 mAh/cm^3). In addition, Mg metal is denser than Li, offering twice the capacity at the same volume. (2) Highly reversible and stable anode. The side reaction between the Mg metal anode and the electrolyte is minimal in ethereal organic electrolytes, leading to reversible Mg deposition/striping for up to 2500 cycles.[17] Such an advantage promises a stable anode/electrolyte interface and ensures a long cycle life.

Organic redox-active molecules are of particular interest as charge carriers in RFBs thanks to their natural abundance, molecular diversity, and structural tunability.[18,19] Their functional groups are easily modified to adjust physical and electrochemical properties such as solubility, chemical stability, redox potential, and kinetics.[20] So far, most organic cathode molecules are explored in acetonitrile (AN)-based electrolytes because they can provide high conductivity and wide potential windows.[21] However, AN is not compatible with Mg metal anode due to its high reactivity.

View Article Online
DOI: 10.1039/D5SC04532K

Another design challenge for organic redox-active molecules in Mg RFBs roots in the instability of soluble cathode and/or charged cathode with Mg anode. Therefore, it is key to finding suitable organic material which is compatible with Mg anode and ethereal electrolytes. Considering the energy density equals to $\boldsymbol{n}\times\boldsymbol{C}\times\boldsymbol{F}\times\boldsymbol{V}$ (where $\boldsymbol{n}$ is the number of transferred electrons, $\boldsymbol{C}$ is the concentration of redox-active molecule, $\boldsymbol{F}$ is Faraday's constant, and $\boldsymbol{V}$ is the cell voltage), requirements for high performance organic cathode molecules also include: (1) multi-electron redox reactions; (2) high solubility; (3) high voltage. In consequence, it is crucial to develop a high-voltage and high-capacity catholyte that is compatible with a Mg metal anode to advance nonaqueous Mg RFBs.

In this work, we first comprehensively examined a wide range of organic molecules with different redox-active moieties in Mg battery electrolyte (**Table S1**), identified the best compatible redox-active molecule in nonaqueous Mg RFBs (**Figure 1a-b**), and obtained the key parameters to design a high-performance catholyte (**Figure 1c-d**). After preliminary screening, the amine-based molecule stands out due to its high voltage and high compatibility with Mg electrolyte. As such, to identify the best amine molecules for Mg RFBs, we examined the multiple design freedoms of amine-based catholytes in RFBs, including the influence of redox-active moiety, non-conjugated and π-conjugated structures, and supporting electrolytes. By combining electrochemical tests with spectroscopic characterizations, we evaluated the performance of selective amine-based catholytes in both three-electrode cell and Mg RFBs and correlated their performance with structures and properties (solubilities, transports, kinetics and stabilities). Density functional theory (DFT) simulations and the average inverse aromatic fluctuation index (FLU^{-1}) were conducted to understand the impact of conjugation degree on the oxidation potential. Hansen solubility parameters (HSP) were employed to analyze how molecular conjugation degree and solvent

View Article Online
DOI: 10.1039/D5SC04532K

polarities influence the solubility behavior of organic molecules. Fundamental knowledge of the chemistry-property-performance correlation of this family of catholytes in various supporting electrolytes and metal anodes were obtained to set the foundation for further catholyte engineering.

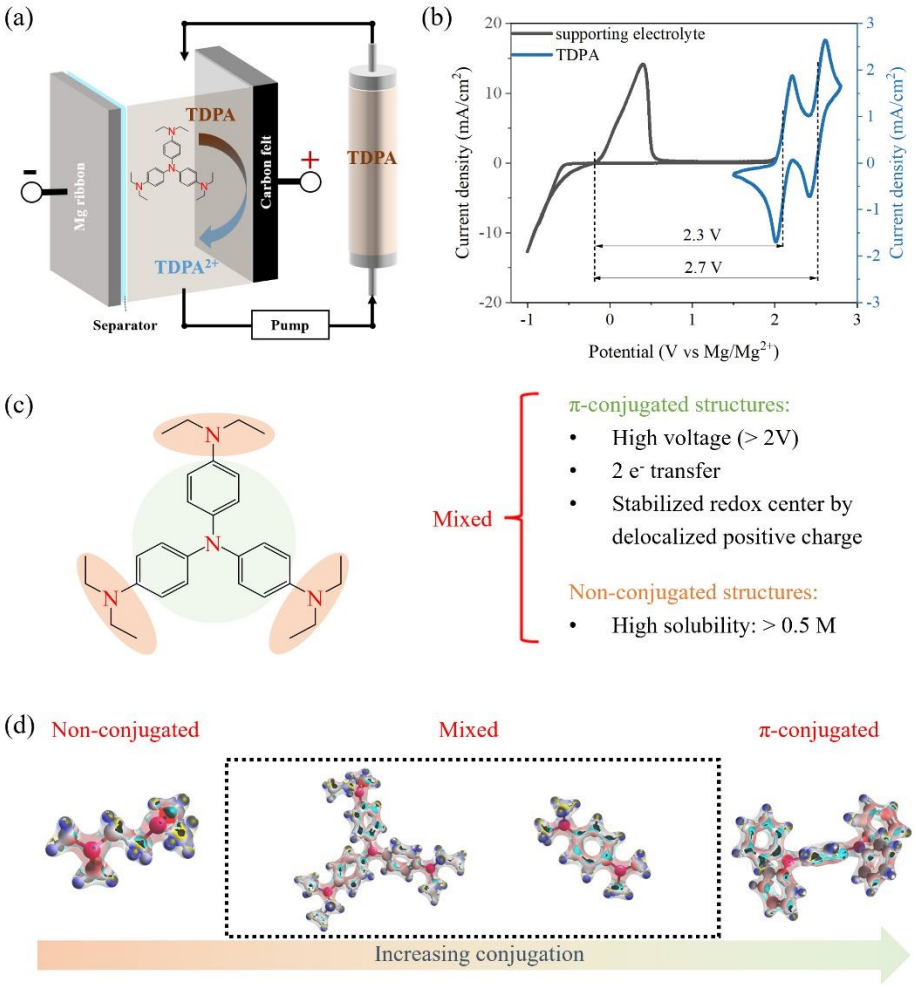

Figure 1. Scope. (a) Schematic diagram of Mg RFBs; (b) CV of the Mg anode and amine-based catholyte; (c) Design principle of amine molecules as the catholyte for Mg RFBs; (d) Electrostatic potential based on the electron density from the natural bond orbital analysis[22] in Gaussian 16[23] package. Figures are rendered using Avogadro software[24]. Red indicates higher charge density and blue indicates lower charge density.

View Article Online
DOI: 10.1039/D5SC04532K

Results

Screening of organic redox moieties for Mg RFBs

To screen the best compatible redox moieties in Mg electrolyte system, we examined the common organic molecules with different redox centers. These molecules include azobenzene (AB, azo), anthraquinone (AQ, quinones), tetrachloro-1,4-benzoquinone (TCBQ, quinones), N,N,N′,N′-tetraphenyl-1,4-phenylenediamine (TPPD, amine), (2,2,6,6-tetramethylpiperidin-1-yl)oxyl (TEMPO, nitroxide radical), 1,10-phenanthroline (Phen, pyridine), diphenyl sulfide (DPS, sulfide) and 1,4-di-tert-butylbenzene (DTBB, dialkoxybenzene) (**Figure 2a** and **Table S1**). Most of these molecules have been demonstrated to exhibit favorable redox activity in other types of flow batteries, while their electrochemical behavior in the context of Mg-based electrolytes deserve investigation.

Azobenzene (AB), composed of two phenyl rings connected by an azo functional group, has demonstrated promising potential for non-aqueous redox flow batteries owing to its high solubility and excellent electrochemical stability.[25] Quinones and its derivates, which contain two or more carbonyl groups connected by conjugation structures, have been widely studied owing to their highly reversible electrochemical redox reactions and fast kinetics.[26,27] Here two types of quinone have been selected, one is anthraquinone (AQ) and the other is tetrachloro-1,4-benzoquinone (TCBQ). AQ consists of an anthracene structure with two carbonyl groups (C=O) at *para* positions. This creates an extended aromatic and conjugated system, enhancing its stability and electrochemical reversibility. TCBQ, on the other hand, has a single benzene ring substituted by two carbonyl groups at *para* positions and four chlorine atoms, which significantly influence their electronic properties by introducing strong electron-withdrawing effects.[28,29] Amines are a class of molecules characterized by C-N bonds. Here, we specifically focus on aromatic amines, composed of phenyl group bonded directly to amine groups. Aromatic amines exhibit several desirable properties for redox flow applications, including ease of functional-group modification (enabling tailored adjustment of redox potential and solubility), and low reorganization energy when converting between neutral and radical forms.[30] In this section, N,N,N′,N′-tetraphenyl-1,4-phenylenediamine (TPPD) is selected as a representative aromatic amine molecule. 2,2,6,6-Tetramethylpiperidin-1-yl)oxyl (TEMPO) is one of the most widely used nitroxide radicals due to

View Article Online
DOI: 10.1039/D5SC04532K

its exceptional stability, which arises from electron delocalization between the nitrogen and oxygen atoms, as well as steric protection provided by the four surrounding methyl groups.[31,32]. Here TEMPO was selected to assess its compatibility with Mg-based electrochemistry. 1,10-phenanthroline (Phen) is commonly used in iron and cobalt redox flow batteries because it can form complexes with metals, thus creating new redox couples.[33,34] Here, we test whether Phen molecules can similarly form complexes with Mg, potentially exhibiting redox activity. Additionally, due to the structural similarity between Phen and amine molecules, which both contain nitrogen atoms bonded to aromatic rings, Phen can serve as a control for amines. Diphenyl sulfide (DPS, a sulfide compound) and 1,4-di-tert-butylbenzene (DTBB, a dialkylbenzene derivative) are aromatic compounds containing benzene rings. In DPS, two phenyl groups are bridged by a sulfur atom, whereas DTBB features tert-butyl substituents on the benzene ring. These molecules were selected to investigate whether sulfur atoms or alkyl chains attached to aromatic systems can exhibit reversible redox activity in Mg-based electrolytes.

View Article Online
DOI: 10.1039/D5SC04532K

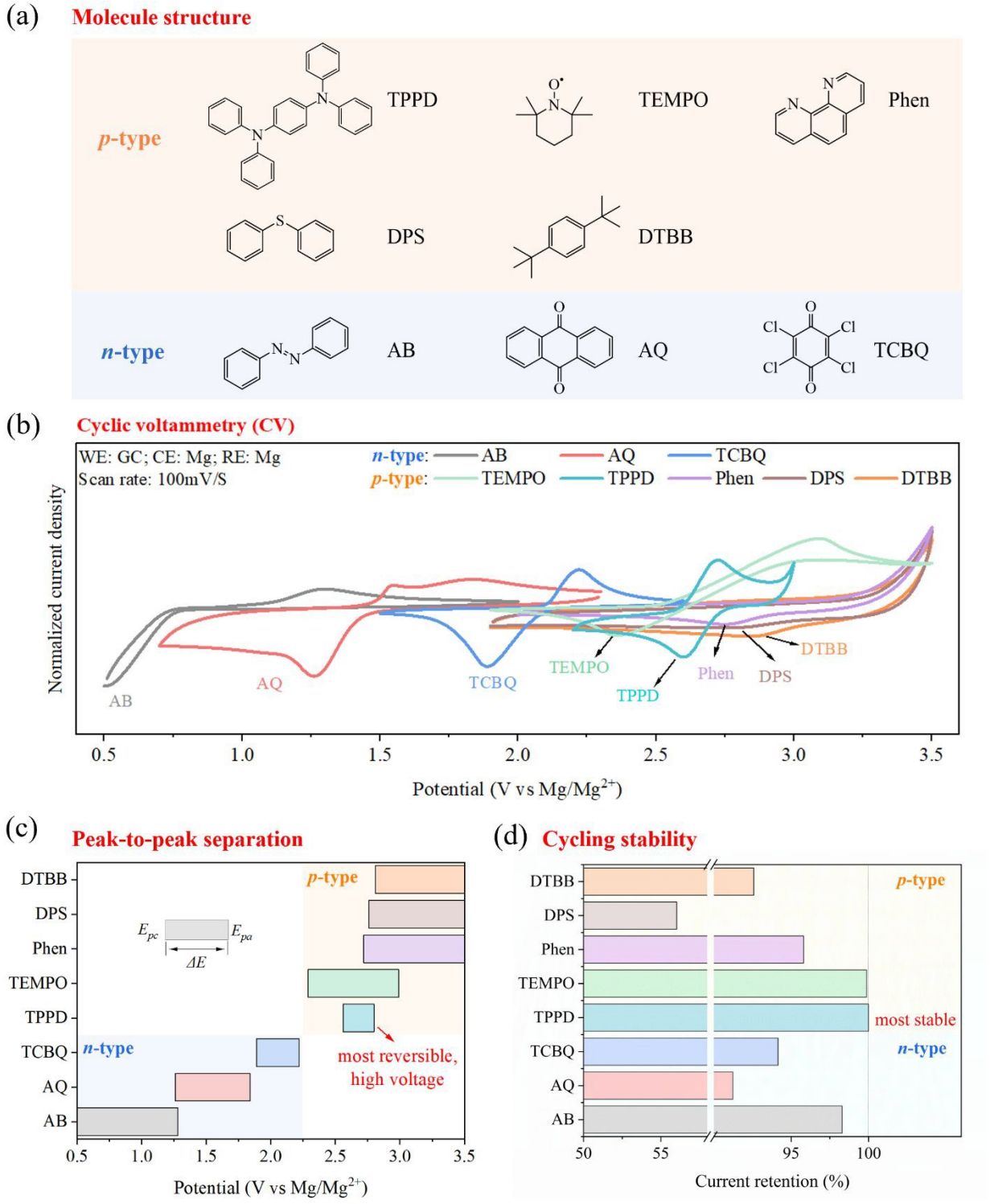

Figure 2. Screening of organic redox moieties for Mg RFBs. (a) Molecule structure of organic molecules with different redox-active moiety; (b) CV profiles, (c) peak-to-peak separation (ΔE)

View Article Online
DOI: 10.1039/D5SC04532K

from CV results, and (d) cycling stabilities of these molecules in Mg electrolyte. The concentration of active materials is set at 1 mmol/l (1mM). Due to variations in solubility among these molecules, this concentration is chosen to ensure a consistent comparison under the same conditions. The Mg electrolyte was prepared by dissolving 0.5 M LiTFSI, 0.25 M Mg powder, and 0.5 M $MgCl_2$ in dimethoxyethane (DME).

According to the different electric charges carried by the redox centers during the electrochemical reactions, these organic molecules can be divided into *p*-type and *n*-type active materials.[35] AB, AQ, and TCBQ belong to *n*-type active materials, carrying negative charges during the charge/discharge processes, while the other molecules belong to *p*-type active materials, carrying positive charges during the charge/discharge processes. Cyclic voltammetry (CV) was conducted to test the redox activities and potentials of these molecules in Mg electrolyte (**Figure 2b**). As summarized in **Figure 2c and Table S2**, *p*-type molecules show higher redox potential (above 2.6 V vs Mg/Mg^{2+}) than *n*-type molecules, which is consistent with literature[36]. Among these molecules, only AQ, TCBQ, TPPD and TEMPO show clear pairs of redox peaks, indicting quinones, amines and nitroxide radical are compatible in Mg chemistry. Their reaction mechanisms were given in Figure S1. Notably, although TEMPO displays reversible redox peaks, it shows a big peak-to-peak separation. As previously reported, Li^+ exhibits a strong solvation interaction with the N–O• site of TEMPO, leading to the formation of a counterion–organic solute pair.[37] Additionally, a peak-to-peak separation of approximately 0.2–0.6 V for TEMPO in a NaClO4–PC electrolyte was reported before.[38] Therefore, the large peak-to-peak separation observed for TEMPO may be attributed to the presence of cations (Mg^{2+} and Li^+) in the electrolyte, which deserves investigation in future work. Reversible redox peaks were not observed for the azo, sulfide, and dialkylbenzene compounds in the Mg electrolyte.

Among these high-potential molecules, TPPD shows the smallest peak-to-peak separation (ΔE), indicating that its redox reaction is most reversible. All the organic molecules, upon oxidation, form radicals or charged species that are stabilized by their conjugated structures (phenyl or N-O bond), resulting in enhanced stability of the charged molecules. The electrochemical stabilities of

View Article Online
DOI: 10.1039/D5SC04532K

these organic molecules (**Figure 2d**) were evaluated by examining the peak current decay during a 300-cycle CV scan and quantified by the peak current ratio of the 300th cycle to the first cycle ($I_{p,300}/I_{p,1}$) (**Figure S2**). TPPD shows the highest stability (100%) compared with the other molecules, demonstrating the stable electron-transfer reaction of the amine group.

In general, amine is the most promising redox-active molecule for Mg RFBs owing to its high redox potential, high reversibility and high stability. In the following study, the influence of its molecular structure on its properties (thermodynamics, solubilities, kinetics, transports and stabilities) was investigated to determine the best structure for amine catholyte design in Mg RFBs.

Establishment of chemistry-properties-performance relationship

Amine moiety stands out from various organic moieties. Previous studies about amines all focused on the para-substituted effect on triphenylamine [30,39–42], while the effect of its π-conjugated and non-conjugated structures has never been explored. Here, four amine molecules (**Figure 3a** and **Table S3**) were chosen to understand how the π-conjugated and/or non-conjugated structures influence the electrochemical performances and other properties of amine-type molecules. TMED is a non-conjugated amine molecule, where the two N atoms are connected to alkyl chains. TPPD is a fully π-conjugated molecule where the two N atoms are connected to phenyl groups. TDPA and TMPD are mixed structures where the two N atoms are both connected with alkyl chains and phenyl groups, simultaneously. Chemical intuition suggests that TPPD has the highest delocalization owing to its highly conjugated structure. However, for the mixed conjugated systems, the situation is more nuanced owing to the presence of delocalizing phenyl and electron withdrawing methyl groups. To quantify this, the average inverse aromatic fluctuation index (FLU^{-1}) of these molecules was calculated in their neutral state (see Methods section). A higher FLU^{-1} value corresponds to stronger aromaticity, indicating a higher electron delocalization. The degree of conjugation follows the sequence: (TMED <) TDPA < TMPD < TPPD (**Figure S3**), with TMED

View Article Online
DOI: 10.1039/D5SC04532K

showing the least conjugation. Although the FLU^{-1} value for TMED is not calculated, it is evident that its conjugation is minimal.

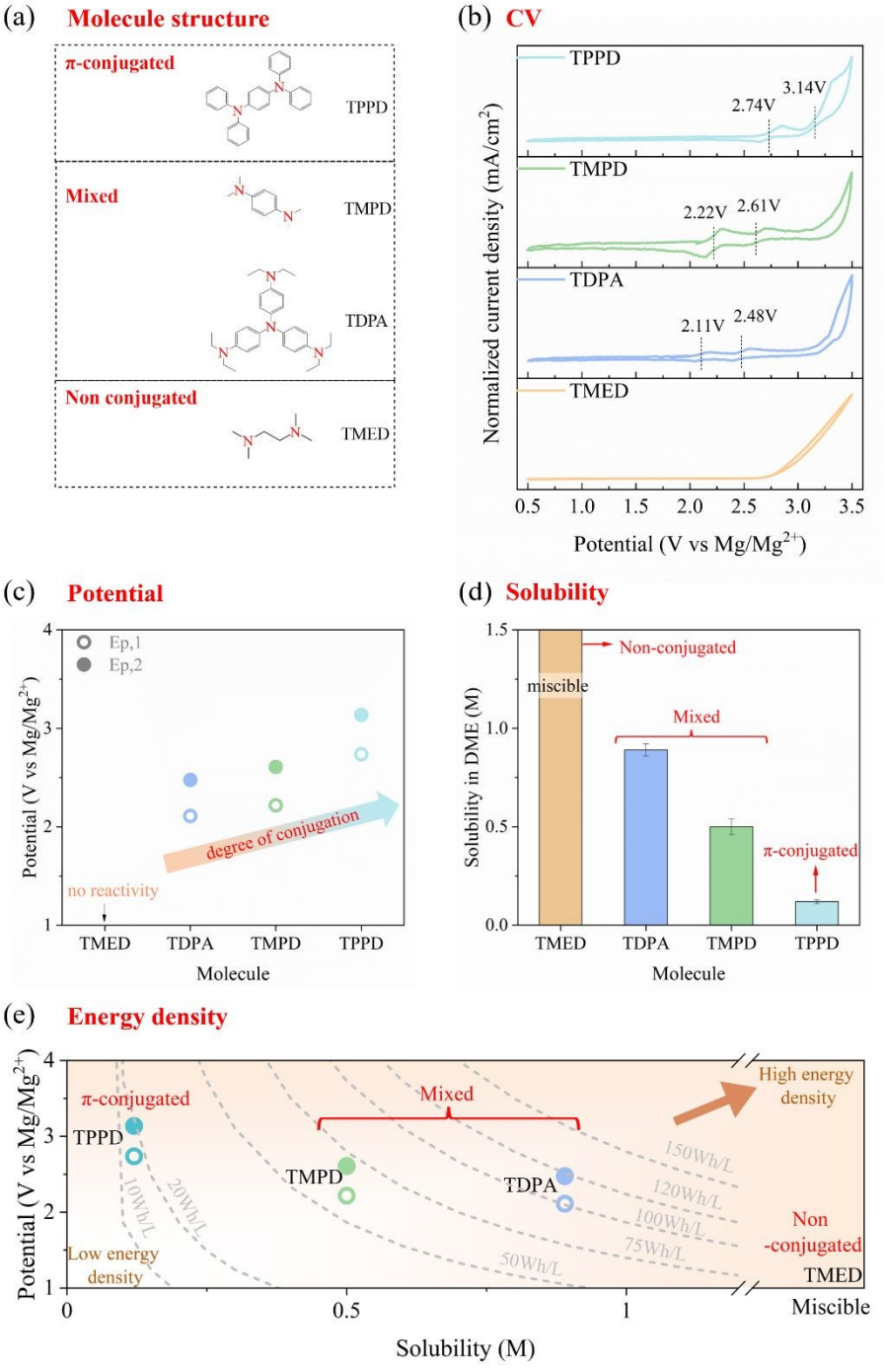

View Article Online
DOI: 10.1039/D5SC04532K

Figure 3. **Structural effect on the electrochemical performances of amine molecules.** (a) Molecular structure, (b) CV profile, (c) potential, (d) solubility and (e) theoretical energy density of different amine molecules in Mg electrolyte. The concentration of active materials is set at 1mM. Note: hollow circles and solid circles represent the first pair of peaks and second pair of peaks, respectively.

As shown in CV profiles (0.5-3.5 V vs Mg/Mg^{2+}) (**Figure 3b**), TMED only shows visible oxidation peak, indicating that molecules with non-conjugated structure have no reversible redox reactivity in this condition. The remaining molecules with π-conjugated structures show two pairs of redox peaks, demonstrating their ability to deliver twice as much capacity compared to one-electron redox couples, such as TEMPO. As their degrees of conjugation increase, their redox potential also increases (**Figure 3c**), demonstrating the electron delocalization in π-conjugated structure are beneficial to achieve high potential. The maximum potential was realized by TPPD at 2.74 V vs Mg/Mg^{2+} for 1st redox reaction and 3.14 V vs Mg/Mg^{2+} for 2nd redox reaction. To understand the origins of the experimental trends, their redox potential and highest occupied molecular orbital (HOMO) (**Figure S4**) were calculated by DFT from their neutral to charged state. The qualitative trends mirror the experimental results. These results highlight the crucial role of conjugation (or electron delocalization) in stabilizing the molecule and decreasing the HOMO energy and increasing redox potential. A molecule with a highly stabilized oxidation state (lower HOMO energy) requires more energy—or a higher redox potential—to undergo oxidation. Noteworthy, the conjugation effect on redox potential of organic molecules relies on its functional group.[43] Organic molecules with conjugating backbones exhibit progressively higher redox potentials as more aromatic rings are incorporated, owing to the strengthened inductive effect. This inductive withdrawal of localized electron density increases the redox potential. For the non-conjugating family, it shows the opposite trend. In our study, the amine function group belongs to the former category because the electron cloud of the lone pair electrons in nitrogen can overlap with and delocalize into the π orbitals of the aromatic ring, resulting in a conjugated structure.[44]

View Article Online
DOI: 10.1039/D5SC04532K

The solubilities of these molecules were tested in DME solutions (**Figure 3d**). The non-conjugated molecule, TMED, is miscible with DME, while the fully π-conjugated molecule, TPPD, shows the lowest solubility (~0.12 M). Molecules with mixed structures exhibit moderate solubilities, ranging from approximately 0.5 to 0.89 M. We compared the Hansen Solubility Parameters (HSP) of dimethoxyethane (DME, the solvent), benzene (used as an approximation for the phenyl group in conjugation structure), methane and ethane (used as an approximation for the alkyl group in non-conjugated structure) (**Table S4**). The δ_D describes dispersion forces and non-polar interactions, δ_P describes polar forces and dipole–dipole interactions, and δ_H describes the hydrogen bonding forces. As the three parameters of the solute and the solvent become more similar, the solubility tends to increase. In the dissolution of amines in the DME system, hydrogen bonding can be disregarded. Given that benzene, ethane, and methane are non-polar molecules and have low ability to form hydrogen bonds, dispersion forces (δ_D) emerge as the primary contributing factor. The $\Delta\delta_D$ difference between benzene and DME (3.0) is significantly larger than that between alkanes and DME (3.0 vs. 1.4 for ethane and 0.1 for methane). As a result, the non-conjugated molecule, TMED, is fully miscible with DME, whereas the fully π-conjugated molecule, TPPD, exhibits the lowest solubility. Other molecules with partial π-conjugation and some alkyl groups display moderate solubility in DME.

Theoretical energy densities were calculated for these molecules (**Figure 3e**). Molecules with mixed structures show theoretical energy densities of 50-120Wh/L, while the theoretical energy densities of non-conjugated molecule and π-conjugated molecules are 0 and ~10 Wh/L due to either low reversible reactivity or low solubility. Overall, mixed structures offer a balance of optimized potential and solubility. Among all the molecules, TDPA demonstrates the most promising performance, achieving a theoretical energy density of approximately 120 Wh/L.

View Article Online
DOI: 10.1039/D5SC04532K

The reaction mechanism was provided in **Figure 4a** using TDPA as an example. It undergoes a 2-electron transfer reaction[45], and two pairs of peaks were obtained for the TDPA/TDPA^{+} and TDPA^{+}/TDPA^{2+} couples, respectively. The mass transport (**Figure 4b**), kinetics (**Figure 4c**) and stabilities (**Figure 4d** and **Figure S5**) of these molecules were evaluated by CV at a 1 mM concentration in Mg electrolyte. The diffusion coefficient D_0 (**Figure S6a-c**) and heterogeneous reduction rate constants k^0 (**Figure S6d-f**) were calculated from cyclic voltammetry data at different scan rates, according to the reported method[46]. The observed diffusion coefficients values are in the range of 3-18×10^{-6} cm^2/s, which is in the same order as the most used organic catholyte molecule in flow batteries (**Figure S6g**). The reaction rates of these amines are lower than that of organic cathode molecules but higher than those of other common inorganic redox couples such as V^{3+}/V^{4+} and Fe^{2+}/Fe^{3+}.[47] The CV curves of TDPA (**Figure 4d**) and TMPD (**Figure S5a**) at the 2nd and 100th cycles at the scan rate of 100 mV/s almost completely overlap with each other, demonstrating the high stabilities of these amine redox couples. It is worth noting that these curves exhibit fluctuations due to the low concentration of active material, which results in a decreased signal-to-noise ratio. To further investigate the effect of concentration, we tested 100 mM TDPA catholyte under the same conditions, as shown in **Figure 4d**. With increased concentration, the CV test displayed smoother profiles. Although the redox potential experienced a slight shift, the stability remained unchanged. For the fully π-conjugated molecule, TPPD, its second redox peak (**Figure S5b**) decay during cycling which may be caused by the electrolyte decomposition at beyond 3.00 V vs Mg/Mg^{2+} (**Figure S5d**). When the up-limit scan range was set to 3.00 V vs Mg/Mg^{2+}, TPPD showed completely overlapping profiles during 100 cycles (**Figure S5c**). The full-range scan, covering both the anode (Mg↔Mg^{2+}) and cathode reactions (e.g., TDPA↔TDPA^{2+}), was conducted at TDPA concentrations of 1 mM, 10 mM, and 100 mM (**Figure**

View Article Online
DOI: 10.1039/D5SC04532K

4e). As the TDPA concentration increases, the current response of the TDPA↔$TDPA^{2+}$ reaction also increases, while the redox potential remains relatively consistent, with only slight shifts observed. Meanwhile, the current response and redox potential of the Mg↔Mg^{2+} reaction were close across different TDPA concentrations. These results indicate that the TDPA and Mg reactions do not interfere with each other. Generally, amine molecules show the high diffusivities, moderate kinetics and high stabilities in Mg electrolytes system, implying that they are favorable for low-polarization, high-efficiency and high-stability Mg RFBs.

View Article Online
DOI: 10.1039/D5SC04532K

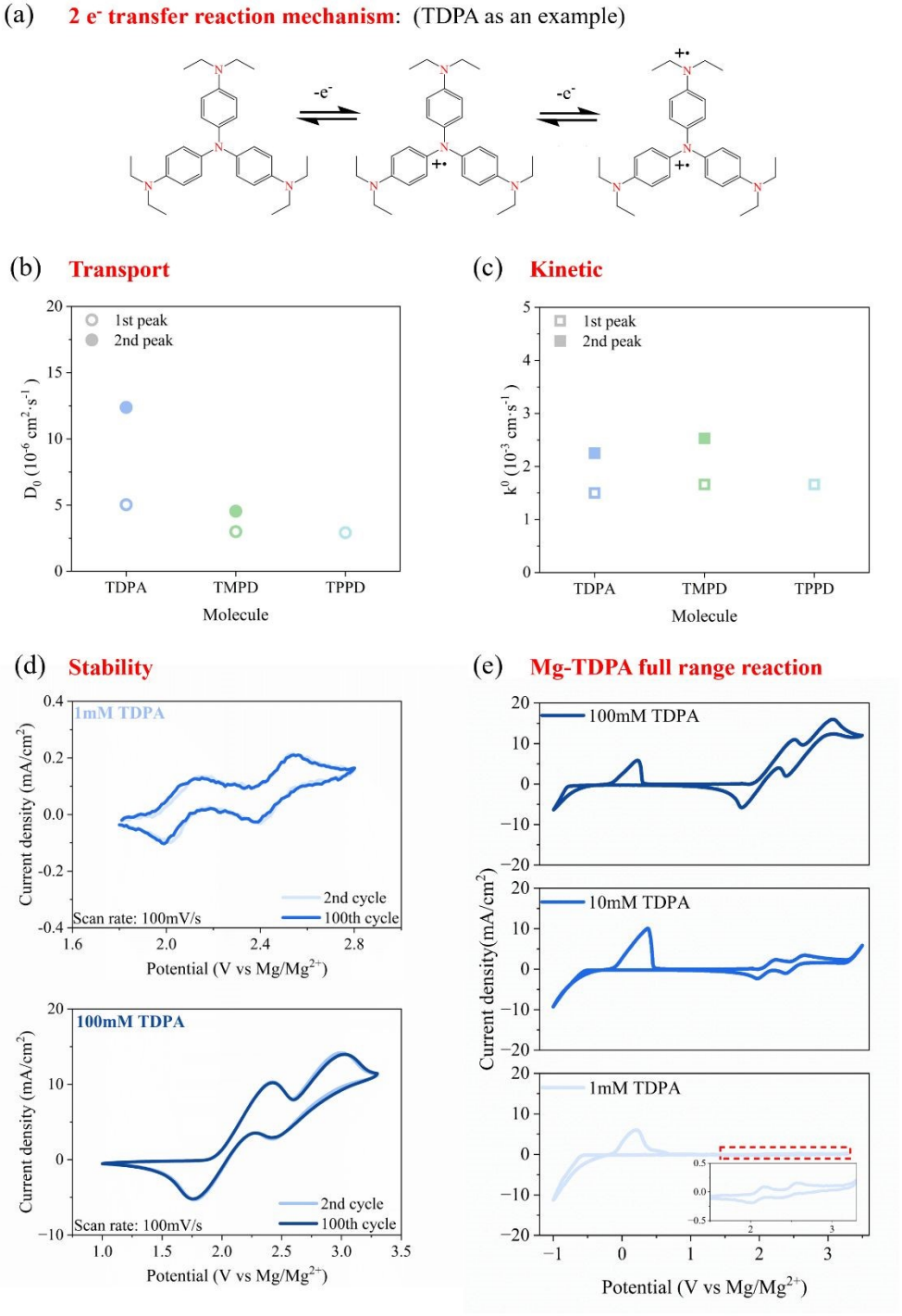

Figure 4. Properties of amine molecules. (a) Reaction mechanism, (b) transport and (c) kinetics. (d) Stability of the TDPA with different TDPA concentrations. (e) CV profiles of Mg-TDPA in full range with different TDPA concentrations.

View Article Online
DOI: 10.1039/D5SC04532K

Mg flow battery demonstration

To confirm the exceptional performance for practical applications, we further examined the electrochemical performance of TDPA at the device level in a flow cell. The cell construction was shown in **Figure 5a**, and experiment details can be found in Methods part. The typical CV curves of the electrolyte and TDPA are shown in **Figure 4e**, which demonstrates the feasibility of realizing a flow cell with a high voltage of around 2.70 V. RFBs using Mg ribbons as the anode, a porous membrane as the separator, and TDPA as catholytes redox-active molecule were assembled and galvanostatically discharged/charged. As shown in **Figure 5b**, the Mg-TDPA cell can deliver an average voltage of 2.50 V, a specific discharge capacity of 95.3 mAh/g (calculated by the weight of TDPA molecule) with a first cycle Coulombic efficiency (1st CE) of 69.07%. The low CE was caused by severe crossover of TDPA molecules through porous membrane, which does not pose any barrier for amine molecules to diffuse through. As evidenced in **Figure 5c**, the porous membrane shows significant cross-over within one day, as indicated by the discoloration. Since amine molecules belong to *p*-type molecules, their states are neutral at the discharged state and positively charged at charged state. To block the cross-over of neutral or positively charged TDPA, anion exchange membrane (AEM) was used to replace the porous membrane, and the cross-over test showed it effectively limits cross-over even after 10 days, demonstrating its superior barrier properties. Such a Mg-TDPA cell using AEM membrane can deliver a specific discharge capacity of 106.5 mAh/g (corresponding to a volumetric capacity of 49 mAh/L) and a 1st CE of 90.74% and achieve 93.88% capacity retention after 150 cycles (**Figure 5d**). After disassembling the cell, cycled Mg ribbon was examined with scanning electron microscopy (SEM) and energy dispersive spectroscopy (EDS). As shown in **Figure 5e**, the Mg ribbon surface shows obvious holes, indicating deposition-dissolution of Mg metal. The EDX mapping also shows the signals for Mg.

View Article Online
DOI: 10.1039/D5SC04532K

The signal for N in TDPA molecule is missing in EDX, demonstrating that AEM effectively inhibited the crossover of TDPA. The great cycling stability is consistent with the molecular stability demonstrated in **Figure 2d**, which demonstrates the great potential of amine molecules to construct long-life Mg RFBs.

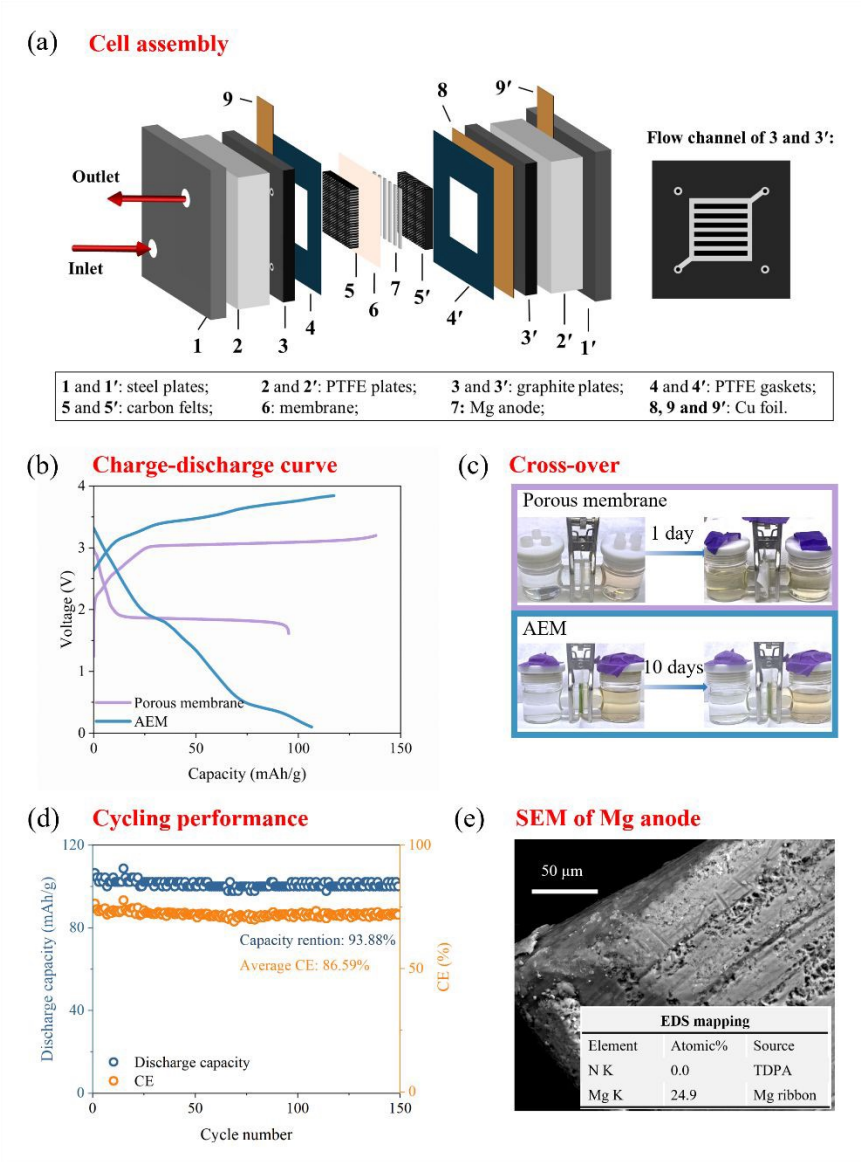

Figure 5. Mg flow battery demonstration: TDPA as example. (a) Cell assembly. (b) Charge-discharge curve. (c) Cross-over of TDPA through porous membrane and AEM. Left side of H-

View Article Online
DOI: 10.1039/D5SC04532K

cell: pure DME; right side of H-cell: 1 mM TDPA in DME. (d) Cycling performance at 10 mA/cm^2. (e) SEM and EDX of Mg ribbon anode after cycling.

The increased overpotential between charge and discharge, along with the low voltage efficiency and energy efficiency (**Figure S7**) is a result of the poor ionic conductivity of the AEM in such non-aqueous electrolytes. Meanwhile, the incomplete CE and slightly chemical change of TDPA catholyte after cycling (**Figure S8**) may be caused by membrane swelling. When using an AEM membrane, the cell exhibits smooth flow when only pumping Mg electrolyte. However, upon adding 0.1 M TDPA, the membrane swells, causing flow disruption at the cell outlet. This indicates that amine molecules interact with AEM, leading to swelling. Notably, this swelling effect diminishes as the concentration decreases. Therefore, in this study, flow cell tests were conducted with low active material concentration, and performance at higher concentrations was not evaluated. It should be noted that the focus of this work is on the design of the organic molecule catholyte for Mg RFBs, whereas the design of highly conductive and high stable ion-selective membrane for non-aqueous flow batteries, despite important, is beyond the scope of the current study.

Electrolyte influence of amine-based catholyte in RFBs

In this work, the electrolyte was prepared by dissolving 0.5 M LiTFSI, 0.25 M Mg powder, and 0.5 M $MgCl_2$ in dimethoxyethane (DME). The active species is $[Mg_2(\mu\text{-}Cl)_2]^{2+}$ cation complex, which is highly active for reversible Mg-based reactions.[48] This complex was formulated in DME through dehalodimerization of non-nucleophilic $MgCl_2$ by reacting with LiTFSI. LiTFSI was chosen over $Mg(TFSI)_2$ due to its higher purity and the absence of any interference from Mg^{2+} ion activity.[49]. Mg powder was added to remove any residue moisture. The effects of electrolyte solvent and salt composition on the amine molecules are unveiled in this section. Since this study primarily focuses on exploring organic cathode molecules that are compatible with Mg anode, the impact of different electrolytes on the redox properties of Mg was not explored in detail.

View Article Online
DOI: 10.1039/D5SC04532K

The catholyte in this work employs a glyme solvent, known for its weak polarity. As mentioned briefly in the Introduction, high-polarity solvents are used in most non-aqueous RFBs to achieve high ionic conductivity of the electrolytes. According to the CV profiles (**Figure S9a**), the choice of solvent does not affect the redox potential of amine-based redox-active molecules. The only difference is that the AN system can achieve higher current density than the DME system due to high conductivity of AN-based supporting electrolyte (**Figure S9b**). To improve the kinetics of TDPA in DME, the flow rate in Mg RFBs can be increased, making conductivity a less critical concern. More importantly, there are two key challenges to using AN/propylene carbonate (PC)-based supporting electrolytes in Mg-amine RFBs (**Figure 6a**): (1) low solubility of amine molecules (**Table S5**) and (2) high reactivity with metal anode. The solubility of TDPA decreases with the increase of solvent polarity. For example, the solubility of TDPA in DME is 16 times and 25 times higher than that in AN and PC, which are the most used solvents in non-aqueous RFBs. As shown in Table S4, the phenyl and alkyl groups in amines have a δ_P value of 0, DME has a moderate δ_P value of 6, while AN and PC have δ_P values of 18. This large difference leads to the extremely low solubility of amines in highly polar solvents. Similar solubility differences can also be observed for TPPD (**Table S6**). Moreover, these high-polarity solvents can react with metal anodes and compromise the stability of Mg RFBs. Based on these, the DME is identified as the best solvent due to its highest solubility and high compatibility with metal anode, which breaks the consensus that high-polarity solvents are necessities in non-aqueous RFBs.

View Article Online
DOI: 10.1039/D5SC04532K

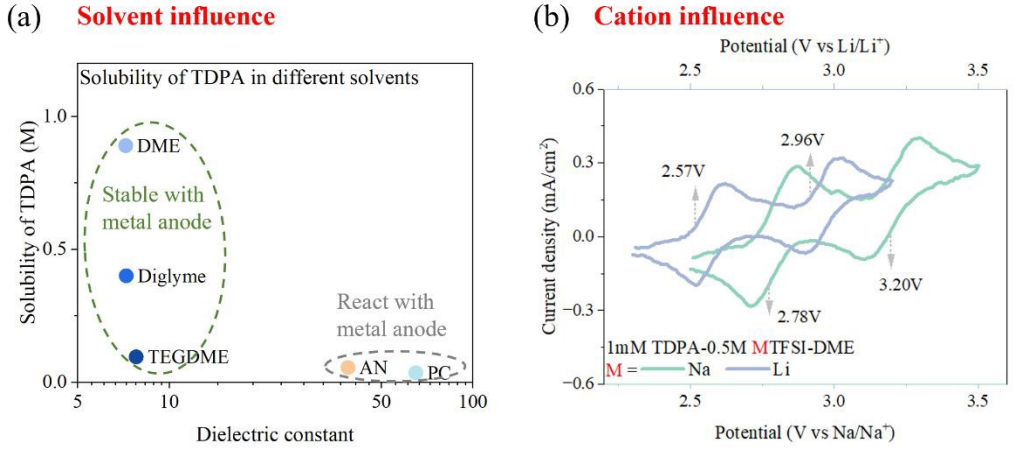

Figure 6. Electrolyte influence. (a) Solubility of TDPA in different solvents with different polarity. (b) CV profiles of 1mM TDPA-DME using different cations.

Additionally, it is worth noting that the amine-based cathode molecule belongs to *p*-type active material. When the amines are oxidized, the positively charged molecules can bond with anions by electrostatic force, and such binding may influence the peak potential. $TFSI^-$ and ClO_4^- were selected here to investigate the bulk anion influence on TDPA performance, and their CV profiles show similar redox peaks (**Figure S10a**). FTIR was conducted to study the chemical bonding environment of TDPA (**Figure S10b**). Compared with pure DME solvent, the profile of TDPA-DME shows a characteristic peak at 1507.121 cm^{-1}, indicating the presence of TDPA. When 0.5M $TFSI^-$ or ClO_4^- are added to the TDPA-DME solution, there is no change of peak position, which means the chemical environment of TDPA was not changed by the anions. Based on the combined electrochemistry and spectroscopy results, we infer that $TFSI^-$ or ClO_4^- ions are only weakly associated with the TDPA molecule and do not significantly influence its redox potential. These amine-based catholytes are also applicable to the Na and Li RFBs (**Figure 6b**) due to the

View Article Online
DOI: 10.1039/D5SC04532K

compatibility of ether with metal anode. In Li-based and Na-based electrolytes, TDPA catholyte also enables two electron transfer reactions (2.57 and 2.96 V vs Li/Li^+, 2.78 and 3.20 V vs Na/Na^+).

Conclusion

Nonaqueous magnesium redox flow batteries (Mg RFBs) are attractive for low-cost, high-energy-density and long-cycle-life stationary energy storage applications. A comprehensive experimental and computational study was conducted to examine organic molecules of different redox moieties and conjugated structures for Mg RFBs. Amine molecules are identified as the best catholyte molecule for Mg RFB due to their high redox potential, excellent reversibility, and superior stability. The critical influence of π-conjugated and non-conjugated structures of amines on their thermodynamics, solubility, kinetics, transport properties, and stability in Mg RFB were systematically studied, highlighting the contribution of this work compared to earlier reports on amine-based flow battery that primarily focused on the para-substituted effects of triphenylamine on redox potential and solubility. [30,39–42]

A key finding of this work is that the redox potential of the amine molecule scales with the degree of conjugation; a higher degree of conjugation results in a higher redox potential of the catholyte. TDPA with mixed π-conjugated and non-conjugated structures show the best performance among all the studied amine molecules due to a balance of optimized potential and solubility. When paired with an Mg anode, a flow battery employing TDPA can achieve energy densities as high as ~120 Wh/L for a concentration of 0.89 M concentration and the observed redox potential of 2.70 V vs Mg/Mg^{2+}. A Mg-amine redox flow battery using TDPA as the catholyte molecule was demonstrated, which delivered a voltage of 2.50 V, a specific discharge capacity of 106.5 mAh/g, an average CE of 86.59%, and achieved 93.88% capacity retention after 150 cycles. This great

View Article Online
DOI: 10.1039/D5SC04532K

performance is attributed to the mixed π-conjugated and non-conjugated structures in TDPA, as well as its high stability and high solubility in the ether-based supporting electrolyte. The cross-over of the amine molecule can be significantly suppressed by replacing porous membrane with AEM at the expense of increasing resistance, overpotential and swelling, highlighting the need of membrane research to fully materialize the potential of Mg RFBs, which is beyond the scope of this work.[50] In addition to non-aqueous Mg RFBs, this class of redox-active molecules are also applicable in various hybrid flow cells such as Li-RFBs and Na-RFBs, expanding the applications and opportunities of amine-based catholytes in flow batteries.

From a molecular design perspective, incorporating more alkyl/glycol chains and phenyl groups into amine-based organic molecules is a promising strategy to enhance the electrochemical performance of amine-based molecules and address cell construction challenges. This strategy has four advantages: Firstly, these organics feature an amine core, as demonstrated in this work, enabling a 2-electron transfer reaction, high voltage, and improved stability. Secondly, their long alkyl chains and/or polyethylene glycol chains (non-conjugated structures) enhance solubility in ether-based solvents. Thirdly, the incorporation of more phenyl groups (π-conjugated structures) increases both stability and redox potential. Lastly, from a cell construction perspective, incorporating more alkyl/glycol chains and phenyl groups ensures a larger molecular size, minimizing crossover through the porous membrane and eliminating the need for high-resistance, easily swelling ion-exchange membranes. Therefore, this work paves the way for rational structure design of organic molecules for Mg-based redox flow batteries.

View Article Online
DOI: 10.1039/D5SC04532K

Methods

Catholyte preparation

All organic molecules used in Figure 2 were listed in Table S1, including their abbreviations, molecular weights, purities and vendors. The four selected anime-based molecules were listed in Table S3 with their properties and vendors. All organic molecules were used as received without further processing. The preparation of the catholytes was conducted by dissolving the cathode molecules in the prepared electrolyte at room temperature without stirring. The supporting electrolytes for Mg RFBs were prepared as follows: 0.5 M of LiTFSI, 0.25 M Mg powder and 0.5 M of $MgCl_2$ were added to DME, and the mixture was stirred for 6 hours at 60 ℃, then the solutions were filtered. The supporting electrolytes for Na RFBs and Li RFBs were prepared by dissolving 0.5 M desired salt in desired solvent. All operations were conducted in a N_2 (99.999%) filled glove box (O_2 <1 ppm and H_2O < 1 ppm).

Magnesium dichloride ($MgCl_2$, 99.99%), Mg powder (50 mesh, >99%), and dimethoxyethane (DME, 99.5%), diglyme (anhydrous, 99.5%), tetraethylene glycol dimethyl ether (TEGDME, >98%), propylene carbonate (PC, 99.7%), and acetonitrile (AN, 99.8%) were purchased from Sigma-Aldrich. Other salts used in this work are sodium perchlorate ($NaClO_4$, 98%, Thermo Scientific Chemicals), sodium bis(trifluoromethanesulfonyl)imide (NaTFSI, 99.5%, Solvionic) and lithium bis(trifluoromethanesulfonyl)imide (LiTFSI, 99.5%, Gotion Inc).

Materials Characterization

Fourier-transform infrared spectroscopy (FTIR) was collected by the Nicolet iS50 FTIR spectrometer with diamond ATR crystal, on which the electrolyte was placed directly on the windows testing holders during the test. Cross-over test was determined using a two-compartment

View Article Online
DOI: 10.1039/D5SC04532K

glass diffusion cell. One compartment was filled with pure DME, and the other was filled with 1 mM TDPA-DME solution. The tested membrane acted as the separator. Scanning electron microscopy (SEM) and energy dispersive spectroscopy (EDS) were collected with an FEI Quanta 600 FEG. Before analysis, samples were washed with DME solvent and dried under vacuum.

Electrochemistry

Cyclic voltammogram (CV) was collected with an Interface 1010 electrochemical workstation from Gamry instruments. To collect the CV of the catholyte, a glass carbon disk (diameter: 3 mm) was used as the working electrode and two polished Mg foils (or Na, Li disks for Na and Li system) were used as the counter electrode and the reference electrode respectively. For catholyte using AN or PC as solvent, Pt was used as counter electrode and Ag/Ag^+ was used as reference electrode. Ag/Ag^+ electrode was filled with 0.01 M $AgBF_4$ -0.5 M $TBAPF_6$ in AN.

Galvanostatic discharge-charge measurements were performed on a multi-channel battery tester made by Landt Instruments. The cell construction can be found in Figure 5a. Porous membrane (pore size: 0.034 μm, Shenzhen Jialiye Technology Co., Ltd) and anion exchange membrane (AEM, Fumasep FAS-30, Fuel cell store) were used as separators. In a typical test, the volume of the catholyte was 10 mL, and the battery was galvanostatically charged and discharged at a current density of 10 mA/cm^2 at room temperature. For the cell using porous membrane, we set the cut-off voltage window from 1.6V to 3.2V for the TDPA redox reaction. For the cell using AEM membrane, we set the cut-off voltage window from 0.1V to 3.8V. The larger window is used to compromise the large overpotential caused by the AEM membrane.

Calculation for aromatic fluctuation index

The inverse aromatic fluctuation index (FLU^{-1}) is used to quantify the delocalization index of the benzene rings in the catholyte molecule. FLU[51] is defined as:

View Article Online
DOI: 10.1039/D5SC04532K

$$FLU = \frac{1}{n}\sum_{A-B}^{ring}\left[\left(\frac{V(B)}{V(A)}\right)^{\alpha}\left(\frac{\delta(A,B) - \delta_{ref}(A,B)}{\delta_{ref}(A,B)}\right)\right]^2 \text{,...(1)}$$

$$\alpha = \begin{cases} 1; V(B) > V(A) \\ -1; V(B) \leq V(A) \end{cases}\text{, ...(2)}$$

$$FLU^{-1} = \frac{1}{n_{rings}}\sum_{i=1}^{n_{rings}} FLU_i \text{ , ...(3)}$$

where A and B denote atoms in the ring, n_{rings} represents the number of phenyl rings, n represents the number of carbon atoms in each phenyl ring, and $\delta(A,B)$ and δ_{ref} represent the ring delocalization index and the reference delocalization index value, respectively. FLU is computed for each phenyl ring and FLU^{-1} is calculated as an average across all the rings. Multiwfn[52] software is used to compute the FLU values for all the molecules in their uncharged state.

Density functional theory (DFT) calculations

Density functional theory (DFT) calculations were used to compute the redox potential of the different catholytes in solution. DFT calculations were performed with Gaussian 16 package with the B3LYP/6-31+G(d,f) basis function. Solvent effects were included implicitly using the polarizable continuum model (PCM). While the experiments were performed in glyme, Gaussian 16 package does not have the parameters corresponding to this solvent. Among the available solvents in Gaussian 16 package, we choose diethyl ether which has a structural similarity and a dielectric constant (4.20) like that to glyme (7.20).

HOMO-LUMO

The energy difference between the highest occupied molecular orbital (HOMO) and lowest unoccupied molecular orbital (LUMO) was computed for the uncharged state in solvent. Multiwfn software is used to obtain the HOMO and LUMO energies.

View Article Online
DOI: 10.1039/D5SC04532K

Author contributions

Yunan Qin: conceptualization, data curation, formal analysis, investigation, methodology, validation, visualization, writing – original draft. **Vaidyanathan Sethuraman**: data curation, formal analysis, methodology, software. **Seong-Gyu Choi**: investigation, formal analysis. **Richard Gonzalez**: investigation, formal analysis**. Chengxiang Chen**: investigation, writing – review & editing. **Lei Cheng**: project administration, resources, supervision. **Chao Luo**: conceptualization, funding acquisition, project administration, supervision, writing – review & editing. **Tao Gao**: conceptualization, funding acquisition, project administration, resources, supervision, writing – review & editing.

Conflict of Interest

There are no conflicts to declare.

Acknowledgment

This work was supported by the National Science Foundation under Grant No. 2247407.

Reference

1. Gielen D, Boshell F, Saygin D, Bazilian MD, Wagner N, Gorini R. The role of renewable energy in the global energy transformation. *Energy Strategy Reviews*. 2019;24:38-50. doi:10.1016/j.esr.2019.01.006

2. Ang TZ, Salem M, Kamarol M, Das HS, Nazari MA, Prabaharan N. A comprehensive study of renewable energy sources: Classifications, challenges and suggestions. *Energy Strategy Reviews*. 2022;43. doi:10.1016/j.esr.2022.100939

View Article Online
DOI: 10.1039/D5SC04532K

3. Borah R, Hughson FR, Johnston J, Nann T. On battery materials and methods. *Mater Today Adv*. 2020;6. doi:10.1016/j.mtadv.2019.100046

4. Njema GG, Ouma RBO, Kibet JK. A Review on the Recent Advances in Battery Development and Energy Storage Technologies. *Journal of Renewable Energy*. 2024;2024:1-35. doi:10.1155/2024/2329261

5. S S. EIA Expects Explosive Growth in U.S. Battery Storage—Can America Ascend to Dominance?

6. Kebede AA, Coosemans T, Messagie M, et al. Techno-economic analysis of lithium-ion and lead-acid batteries in stationary energy storage application. *J Energy Storage*. 2021;40(June):102748. doi:10.1016/j.est.2021.102748

7. Olivetti EA, Ceder G, Gaustad GG, Fu X. Lithium-Ion Battery Supply Chain Considerations: Analysis of Potential Bottlenecks in Critical Metals. *Joule*. 2017;1(2):229-243. doi:10.1016/j.joule.2017.08.019

8. Noack J, Roznyatovskaya N, Herr T, Fischer P. The Chemistry of Redox-Flow Batteries. *Angewandte Chemie - International Edition*. 2015;54(34):9776-9809. doi:10.1002/anie.201410823

9. Zhang C, Yuan Z, Li X. Designing Better Flow Batteries: An Overview on Fifty Years' Research. *ACS Energy Lett*. 2024;9(7):3456-3473. doi:10.1021/acsenergylett.4c00773

10. Chen H, Xu Y, Liu C, He F, Hu S. Storing Energy in China-An Overview. In: *Storing Energy: With Special Reference to Renewable Energy Sources*. Elsevier Inc.; 2016:509-527. doi:10.1016/B978-0-12-803440-8.00024-5

View Article Online
DOI: 10.1039/D5SC04532K

11. Small LJ, Fujimoto CH, Pratt HD, Anderson TM. *DOE ESHB Chapter 6 Redox Flow Batteries*.; 2021.

12. Chen H, Cong G, Lu YC. Recent progress in organic redox flow batteries: Active materials, electrolytes and membranes. *Journal of Energy Chemistry*. 2018;27(5):1304-1325. doi:10.1016/j.jechem.2018.02.009

13. Gong K, Fang Q, Gu S, Li SFY, Yan Y. Nonaqueous redox-flow batteries: Organic solvents, supporting electrolytes, and redox pairs. *Energy Environ Sci*. 2015;8(12):3515-3530. doi:10.1039/c5ee02341f

14. Qin Y, Holguin K, Fehlau D, Luo C, Gao T. Nonaqueous Mg Flow Battery with a Polymer Catholyte. *ACS Appl Energy Mater*. 2022;5(3):2675-2678. doi:10.1021/acsaem.2c00363

15. Qin Y, Holguin K, Fehlau D, Luo C, Gao T. Exploring Carbonyl Chemistry in Non-aqueous Mg Flow Batteries. *Chem Asian J*. 2022;17(21). doi:10.1002/asia.202200587

16. Gautam RK, McGrath JJ, Wang X, Jiang JJ. Air-Stable Membrane-Free Magnesium Redox Flow Batteries. *J Am Chem Soc*. Published online 2024. doi:10.1021/jacs.4c10106

17. Dong H, Liang Y, Tutusaus O, et al. Directing Mg-Storage Chemistry in Organic Polymers toward High-Energy Mg Batteries. *Joule*. 2019;3(3):782-793. doi:10.1016/j.joule.2018.11.022

18. Ding Y, Zhang C, Zhang L, Zhou Y, Yu G. Pathways to Widespread Applications: Development of Redox Flow Batteries Based on New Chemistries. *Chem*. 2019;5(8):1964-1987. doi:10.1016/j.chempr.2019.05.010

View Article Online
DOI: 10.1039/D5SC04532K

19. Zhang L, Qian Y, Feng R, et al. Reversible redox chemistry in azobenzene-based organic molecules for high-capacity and long-life nonaqueous redox flow batteries. doi:10.1038/s41467-020-17662-y

20. Fang X, Li Z, Zhao Y, Yue D, Zhang L, Wei X. Multielectron Organic Redoxmers for Energy-Dense Redox Flow Batteries. *ACS Mater Lett*. Published online 2022. doi:10.1021/acsmaterialslett.1c00668

21. Izutsu K. *Electrochemistry in Nonaqueous Solutions*. 2nd ed. John Wiley & Sons; 2009.

22. Glendening ED, Reed AE, Carpenter JE, Weinhold F. NBO Version 3.1. *TCI, University of Wisconsin, Madison*. 1998;65.

23. Frisch MJ, Trucks GW, Schlegel HB, et al. Gaussian 16 Rev. C.01. Published online 2016.

24. Hanwell MD, Curtis DE, Lonie DC, Vandermeersch T, Zurek E, Hutchison GR. Avogadro: an advanced semantic chemical editor, visualization, and analysis platform. *J Cheminform*. 2012;4(1):17. doi:10.1186/1758-2946-4-17

25. Zhang L, Qian Y, Feng R, et al. Reversible redox chemistry in azobenzene-based organic molecules for high-capacity and long-life nonaqueous redox flow batteries. *Nat Commun*. 2020;11(1):1-11. doi:10.1038/s41467-020-17662-y

26. Son EJ, Kim JH, Kim K, Park CB. Quinone and its derivatives for energy harvesting and storage materials. *J Mater Chem A Mater*. 2016;4(29):11179-11202. doi:10.1039/c6ta03123d

View Article Online
DOI: 10.1039/D5SC04532K

27. Wang W, Xu W, Cosimbescu L, Choi D, Li L, Yang Z. Anthraquinone with tailored structure for a nonaqueous metal-organic redox flow batter. *Chemical Communications*. 2012;48(53):6669-6671. doi:10.1039/c2cc32466k

28. Hamenu L, Madzvamuse A, Mohammed L, et al. Highly stable 2,3,5,6-tetrachloro-1,4-benzoquinone electrodes for supercapacitors. *Synth Met*. 2017;231:25-33. doi:10.1016/j.synthmet.2017.06.006

29. Bartak DE, Osteryoung RA. *The Redox Behavior of the Tetrachloro-p-Benzoquinone-Tetrachlorohydroquinone System in Molten Aluminum Chloride-Sodium Chloride Solvents*. Vol 74.; 1976.

30. Farag NL, Jethwa RB, Beardmore AE, et al. Triarylamines as Catholytes in Aqueous Organic Redox Flow Batteries. *ChemSusChem*. 2023;16(13):1-9. doi:10.1002/cssc.202300128

31. Pan F, Wang Q. Redox species of redox flow batteries: A review. *Molecules*. 2015;20(11):20499-20517. doi:10.3390/molecules201119711

32. Singh V, Kim S, Kang J, Byon HR. Aqueous organic redox flow batteries. *Nano Res*. 2019;12(9):1988-2001. doi:10.1007/s12274-019-2355-2

33. Hannonen J, Tuna A, Gonzalez G, Martínez González E, Peljo P. Investigation of Fe(II) Complexes with 1,10-Phenanthroline and 2,2′;6′,2“-Terpyridine for Aqueous Flow Battery Applications. *ChemElectroChem*. 2025;12(5). doi:10.1002/celc.202400574

View Article Online
DOI: 10.1039/D5SC04532K

34. Xing X, Zhang D, Li Y. A non-aqueous all-cobalt redox flow battery using 1,10-phenanthrolinecobalt(II) hexafluorophosphate as active species. *J Power Sources*. 2015;279:205-209. doi:10.1016/j.jpowsour.2015.01.011

35. Hatakeyama-Sato K, Oyaizu K. Redox: Organic Robust Radicals and Their Polymers for Energy Conversion/Storage Devices. *Chem Rev*. 2023;123(19):11336-11391. doi:10.1021/acs.chemrev.3c00172

36. Muench S, Wild A, Friebe C, Häupler B, Janoschka T, Schubert US. Polymer-Based Organic Batteries. *Chem Rev*. 2016;116(16):9438-9484. doi:10.1021/acs.chemrev.6b00070

37. Chen R. Toward High-Voltage, Energy-Dense, and Durable Aqueous Organic Redox Flow Batteries: Role of the Supporting Electrolytes. *ChemElectroChem*. 2019;6(3):603-612. doi:10.1002/celc.201801505

38. Yu X, Yu WA, Manthiram A. High-Energy, Single-Ion-Mediated Nonaqueous Zinc-TEMPO Redox Flow Battery. *ACS Appl Mater Interfaces*. 2020;12(43):48654-48661. doi:10.1021/acsami.0c14736

39. Kwon G, Lee K, Yoo J, et al. Highly persistent triphenylamine-based catholyte for durable organic redox flow batteries. *Energy Storage Mater*. 2021;42(April):185-192. doi:10.1016/j.ensm.2021.07.006

40. Romadina EI, Volodin IA, Stevenson KJ, Troshin PA. New highly soluble triarylamine-based materials as promising catholytes for redox flow batteries. *J Mater Chem A Mater*. 2021;9(13):8303-8307. doi:10.1039/d0ta11860e

View Article Online
DOI: 10.1039/D5SC04532K

41. Kim H seung, Lee KJ, Han YK, Ryu JH, Oh SM. A comparative study on the solubility and stability of p-phenylenediamine-based organic redox couples for non-aqueous flow batteries. *J Power Sources*. 2017;348:264-269. doi:10.1016/j.jpowsour.2017.03.019

42. Wang X, Tang W, Loh KP. Para-Substituted Triphenylamine as a Catholyte for Zinc-Organic Aqueous Redox Flow Batteries. *ACS Appl Energy Mater*. 2021;4(4):3612-3621. doi:10.1021/acsaem.1c00031

43. Jung KH, Jeong GS, Go CY, Kim KC. Conjugacy of organic cathode materials for high-potential lithium-ion batteries: Carbonitriles versus quinones. *Energy Storage Mater*. 2020;24:237-246. doi:10.1016/j.ensm.2019.08.014

44. Dai G, Wang X, Qian Y, et al. Manipulation of conjugation to stabilize N redox-active centers for the design of high-voltage organic battery cathode. *Energy Storage Mater*. 2019;16:236-242. doi:10.1016/j.ensm.2018.06.005

45. Kundu D, Black R, Adams B, Nazar LF. A highly active low voltage redox mediator for enhanced rechargeability of lithium-oxygen batteries. *ACS Cent Sci*. 2015;1(9):510-515. doi:10.1021/acscentsci.5b00267

46. Wang H, Sayed ⊥, Sayed Y, et al. Redox Flow Batteries: How to Determine Electrochemical Kinetic Parameters. *ACS Nano*. 2020;14. doi:10.1021/acsnano.0c01281

47. Weber AZ, Mench MM, Meyers JP, Ross PN, Gostick JT, Liu Q. Redox flow batteries: A review. *J Appl Electrochem*. 2011;41(10):1137-1164. doi:10.1007/s10800-011-0348-2

View Article Online
DOI: 10.1039/D5SC04532K

48. Cheng Y, Stolley RM, Han KS, et al. Highly active electrolytes for rechargeable Mg batteries based on a [Mg2(μ-Cl)2]2+ cation complex in dimethoxyethane. *Physical Chemistry Chemical Physics*. 2015;17(20):13307-13314. doi:10.1039/c5cp00859j

49. Shterenberg I, Salama M, Yoo HD, et al. Evaluation of (CF 3 SO 2) 2 N − (TFSI) Based Electrolyte Solutions for Mg Batteries . *J Electrochem Soc*. 2015;162(13):A7118-A7128. doi:10.1149/2.0161513jes

50. MacHado CA, Brown GO, Yang R, Hopkins TE, Pribyl JG, Epps TH. Redox Flow Battery Membranes: Improving Battery Performance by Leveraging Structure-Property Relationships. *ACS Energy Lett*. 2021;6(1):158-176. doi:10.1021/acsenergylett.0c02205

51. Matito E, Duran M, Solà M. The aromatic fluctuation index (FLU): A new aromaticity index based on electron delocalization. *Journal of Chemical Physics*. 2005;122(1). doi:10.1063/1.1824895

52. Lu T, Chen F. Multiwfn: A multifunctional wavefunction analyzer. *J Comput Chem*. 2012;33(5):580-592. doi:10.1002/jcc.22885

View Article Online
DOI: 10.1039/D5SC04532K

The data supporting this article have been included as part of the Supplementary Information.